AGU
ADVANCING EARTH AND SPACE SCIENCES

Geophysical Research Letters®

Key Points:

- For the same velocity, cores with pneumatophores had higher turbulent kinetic energy (TKE) compared to cores without pneumatophores
- Unlike sands, the inception of erosion and erosion rates for cohesive sediment were better predicted by bed shear stress than by TKE
- Modelers should parameterize erosion within vegetation differently for cohesive and non-cohesive sediment

Supporting Information:

Supporting Information may be found in the online version of this article.

Correspondence to:

H. Nepf,
hmnepf@mit.edu

Vegetation-Generated Turbulence Does Not Impact the Erosion of Natural Cohesive Sediment

Autumn R. Deitrick[1,2] [ID], **David K. Ralston**[3] [ID], **Christopher R. Esposito**[4] [ID], **Melissa M. Baustian**[5] [ID], **Maricel Beltrán Burgos**[4] [ID], **Andrew J. Courtois**[4], and **Heidi Nepf**[1] [ID]

[1]Civil and Environmental Engineering, M.I.T, Cambridge, MA, USA, [2]MIT-WHOI Joint Program in Oceanography/Applied Ocean Science and Engineering, Cambridge and Woods Hole, MA, USA, [3]Department of Applied Ocean Physics and Engineering, Woods Hole Oceanographic Institution, Woods Hole, MA, USA, [4]The Water Institute, Baton Rouge, LA, USA, [5]U.S. Geological Survey Wetland and Aquatic Research Center, Baton Rouge, LA, United States, Previously at the Water Institute, Baton Rouge, LA, USA

Abstract Previous studies have demonstrated that vegetation-generated turbulence can enhance erosion rate and reduce the velocity threshold for erosion of non-cohesive sediment. This study considered whether vegetation-generated turbulence had a similar influence on natural cohesive sediment. Cores were collected from a black mangrove forest with aboveground biomass and exposed to stepwise increases in velocity. Erosion was recorded through suspended sediment concentration. For the same velocity, cores with pneumatophores had elevated turbulent kinetic energy compared to bare cores without pneumatophores. However, the vegetation-generated turbulence did not increase bed stress or the rate of resuspension, relative to bare cores. It was hypothesized that the short time-scale fluctuations associated with vegetation-generated turbulence were not of sufficient duration to break cohesion between grains, explaining why elevated levels of turbulence associated with the pneumatophores had no impact on the erosion threshold or rate.

Plain Language Summary Mangrove habitat grows by retaining sediment. To restore these systems, it is necessary to understand how vegetation influences the transport and retention of sediment. This study used sediment cores collected from the interior of a mangrove forest to study how the aboveground roots, called pneumatophores, influence hydrodynamic conditions and sediment transport, and in particular the onset and rate of sediment erosion. Individual pneumatophores generate eddies that enhance turbulence, compared to conditions without pneumatophores. In sandy soil, vegetation-generated turbulence can enhance erosion. However, in this study, vegetation-generated turbulence did not increase the rate of erosion for natural cohesive (muddy) sediment, suggesting that the mangrove forest interior has naturally greater resistance to erosion and sediment loss.

1. Introduction

Coastal vegetation, such as marsh and mangrove, provide valuable ecosystem services. For example, both marsh and mangrove habitats have been shown to reduce property damage and loss of life associated with coastal storms (Das & Vincent, 2009; Hochard et al., 2019; Narayan et al., 2017). Aquatic vegetation also creates low-energy habitats that are important to coastal fisheries (Costanza et al., 1997; Jessup et al., 2021) and are hotspots for carbon sequestration (Macreadie et al., 2021; Mcleod et al., 2011). Recognition of these benefits has accelerated the conservation and restoration of these coastal ecosystems worldwide (Waltham et al., 2020).

Mangrove and marsh habitats are maintained and grow, in large part, through their ability to retain and accrete sediment. Therefore, to restore these ecosystems, it is necessary to understand how vegetation influences the transport and retention of sediment (Cox et al., 2022; Mullarney et al., 2017; Paola et al., 2011). The hydrodynamic drag associated with vegetation reduces currents, which has been associated with enhanced sediment deposition (e.g., Abt et al., 1994). However, vegetation also generates turbulence, which can alter the vertical distribution of suspended sediment (Norris et al., 2021; Tseng & Tinoco, 2021; Xu et al., 2022). For non-cohesive sediment, vegetation-generated turbulence both reduces the critical velocity at which resuspension is initiated (Tang et al., 2019; Tinoco & Coco, 2016, 2018) and, once initiated, enhances the rate of erosion (Xu et al., 2022). Vegetation-generated turbulence enhances erosion in two ways: (a) by mixing momentum toward the bed, which increases bed stress (Conde-Frias et al., 2023; Liu et al., 2008), and (b) by directly interacting with the bed and mobilizing sediment with enhanced instantaneous shear and normal stresses (Celik et al., 2010). However, for

Writing – original draft: Autumn R. Deitrick, Heidi Nepf
Writing – review & editing: David K. Ralston, Christopher R. Esposito, Maricel Beltrán Burgos, Heidi Nepf

non-cohesive sediment, the enhancement in mean bed shear stress is not sufficient to explain the enhancement in erosion rate, indicating that the direct influence of turbulence on resuspension plays the dominant role is setting erosion rates (Xu et al., 2022). Enhanced erosion within finite patches of vegetation has been observed to reduce bed elevation, relative to surrounding substrate (Bouma et al., 2007; Follett & Nepf, 2012). In a mangrove forest fringe, Norris et al. (2021) measured higher turbulence in regions with a greater density of pneumatophores (above ground roots), and these regions were associated with lower topography, which was attributed to pneumatophore-generated turbulence enhancing sediment transport.

The previous field and laboratory studies showing that erosion is enhanced by vegetation-generated turbulence (summarized in previous paragraph) primarily considered non-cohesive sediment. However, cohesion is also important in the erosion process. Cohesion can arise from the presence of fine grain sizes and organics (e.g., Lamb et al., 2020; Wu et al., 2018). Sediment cohesion can also arise from bio-stabilization. Sediment often contains organisms (e.g., bacteria, diatoms, and polychetes) that produce extracellular polymeric substances (EPS) that enhance sediment cohesion (Grabowski et al., 2011; Tolhurst et al., 2008; Valentine et al., 2014; Widdows et al., 2004). In particular, the bridging of grains by EPS eliminates the rolling grain motion commonly observed at the initiation of non-cohesive sediment motion (Packman, 2013).

The purpose of this study was to observe whether, or not, vegetation-generated turbulence impacted the erosion threshold and erosion rate of natural cohesive sediment retrieved from the interior of a mangrove forest. Cores with and without pneumatophores were separately exposed to the same sequence of velocity. Although vegetation-generated turbulence significantly enhanced turbulence levels over the sediment core, measured rates of erosion were similar between cores with and without pneumatophores, suggesting that vegetation-turbulence differently impacts cohesive and non-cohesive sediment erosion.

2. Materials and Methods

Sediment cores were collected at two black mangrove (*Avicennia germinans*) sites in Port Fourchon, Louisiana, USA, during February 2022 (Figure S1 in Supporting Information S1). Two cores with pneumatophores were collected at each site. Two sediment cores were also collected from a tidal channel (≈2 m width and ≈1.5 m depth) at Site *A* (Figure S2 in Supporting Information S1). The channel cores had no aboveground or belowground roots. At each site, grain size analysis was done on sediment samples collected from the top 2 cm (Table 1; Table S1 in Supporting Information S1).

To collect a sediment core, a four-sided acrylic box (20 cm outer side length, 18.4 cm inner side length, and 15 cm depth) was placed on the sediment surface. A shovel was used to dig around the box to 30-cm depth. The box was pushed down until its top was at the soil surface. A rope saw was used to cut through the belowground biomass beneath the core. After the core was removed, a custom-made rubber gasket was placed on the bottom of the box to secure the sample. Prior to shipment to the Massachusetts Institute of Technology (MIT), the cores were stored in a laboratory at the University of New Orleans for a week. The cores were regularly misted with water to keep the soil surface damp, and black plastic covers were placed over each core to prevent light from stimulating microbial activity. Once the cores arrived at MIT, each core was placed in a 30-L salt-water bath with a salinity of 15 ppt, based on salinity measured in the field during retrieval. The water was stirred daily and replaced weekly.

Experiments were conducted in a recirculating Plexiglas channel with a 283 cm x 20 cm x 39 cm working section (Figure 1; Figures S3, S4 in Supporting Information S1). A Plexiglas box (solid red line) with a ramp at the upstream end (dashed red line, Figure 1) raised the flume bed. A core was inserted midway along this raised section, shown as a brown box in Figure 1. Square acrylic plates (18 cm x 18 cm x 0.8 cm) were placed beneath the core to push it upward until its surface was flush with the raised test section bed. The water depth, measured at the downstream end of the flume, was $H = 10$ cm. A 5-cm high, sharp-crested weir at the downstream end of the flume was used to fix the water depth.

To investigate the influence of vegetation-generated turbulence, the pneumatophores were removed from one side of the core. The characteristics of the pneumatophores on the unaltered side of the core are shown in Table 1. A plexiglass frame consisting of four walls in a trapezoid shape was inserted flush with the core surface (gray lines in Figure 1 Top View; photograph in Figure S4 in Supporting Information S1). The structure divided the channel such that half of the core surface was exposed to unidirectional flow and half was completely protected from flow, with no flow leakage between the sections. The resulting test section width (10 cm) was large compared to the
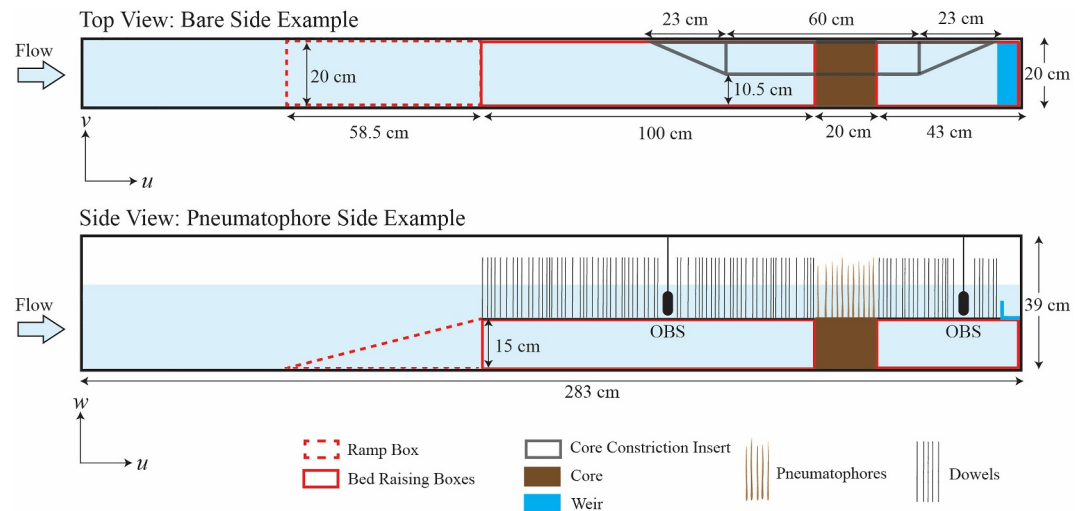
Figure 1. In the Top View the channel is set up for a bare core test. Gray lines show the plexiglass frame that divided the channel such that half of the core was exposed to unidirectional flow and half was completely protected from flow. In the Side View the channel is set-up for a test with pneumatophores. Arrays of circular dowels were placed upstream and downstream of core to mimic surrounding pneumatophores present in the field. See Figures S3 and S4 in Supporting Information S1 for photographs.

pneumatophore diameter (0.65 cm), and the distance between individual roots was comparable to the distance between the roots and the wall, both of which were large compared to the root diameter. Given these conditions, the shedding of turbulence from individual plants was not influenced by channel width.

Experiments exposing the ½ core surface with and ½ core surface without pneumatophores were run separately and in succession. For experiments with pneumatophores, the flow upstream and downstream of the core was conditioned by an array of emergent cylindrical dowels, which mimicked the influence of surrounding pneumatophores that would be present in the field. The dowel diameter, 0.6 cm, was chosen to match the pneumatophore diameter, and the dowel solid volume fraction (SVF) was matched to the core (Table 1). A random array generator code (MATLAB) was used to determine the positions of the dowels.

For each experiment, the core was exposed to stepwise increases in channel-average velocity from 0 to 0.6 m/s. The channel-average velocity ($U_o = Q/A_c$) was calculated from the flow meter reading, Q, and the cross-sectional area of flow above the core A_c. Before each experiment (i.e., for $U_o = 0$ cm/s), a background water sample was taken at the upstream and downstream end of the flume. Next, the pump speed was slowly increased to the first desired velocity. Suspended sediment concentration (SSC) was measured using two optical backscatter sensors (OBS, Seapoint Sensors, Inc.), located upstream and downstream of the core (Figure 1 side view). Each OBS was mounted vertically against the wall and directed across the channel at mid-depth. Since

Table 1
Characteristics of Sediment and Black Mangrove Pneumatophores

Site	D_{50} (μm)	C_f	Core	N	d_{avg} (cm)	ϕ
A	14.1 ± 0.6	0.0019 ± 0.0010	A1	10	0.61 ± 0.03	0.0173 ± 0.0011
			A2	22	0.65 ± 0.02	0.043 ± 0.002
C	28 ± 3	0.0020 ± 0.0002	C1	19	0.47 ± 0.03	0.020 ± 0.002
			C2	24	0.43 ± 0.02	0.022 ± 0.002
Channel	26	0.0013 ± 0.0006	Na	0	Na	Na

Note. See Section S2 in Supporting Information S1 for grain size analysis. Only one sediment sample was analyzed from channel. C_f is bed friction coefficient. The number of pneumatophores (N) and average diameter, d_{avg}, are from the side of core tested with pneumatophores, which had surface area $A_{core} = 169$ cm^2. The pneumatophore area density $n = N/A_{core}$. The solid volume fraction $\phi = \frac{\pi}{4} n d_{avg}^2$.

the OBS has a 2.5 cm diameter, the sensing volume extended from $y = 2.5$ to 7.5 cm, covering the central portion of the channel. Once in suspension, the sediment was mixed each time it passed through the pump. Since this occurred over time scales of minutes, which was much shorter than the time scale for settling (hours), the vertical profile of SSC was uniform (Deitrick et al., 2023), so that OBS measurements at mid-depth were representative of the depth average. It is important to note that this is a function of the experimental facility, and not a function of the presence or density of pneumatophores, and it cannot be generalized to other studies. Once the OBS voltage stopped increasing with time, indicating that all sediment that could erode at this pump speed had been eroded, additional water samples were taken at the up- and downstream ends of the flume, and the process was repeated at the next pump speed. After each experiment, the core was carefully removed from the flume and placed back in a 30 L salt-water bath. The flume was cleaned and prepared for the next experiment. The methodology for these erosion experiments was adapted from Widdows et al. (2008).

The water samples were filtered through pre-weighed 0.7-μm pore size, 47-mm diameter glass fiber filters, which were dried in a 60°C oven for 4 hr, which was sufficient to reach a constant weight. The change in filter mass and sample water volume were used to calculate SSC. The OBS voltage at the time of water sampling was averaged over the 30 s it took to collect the water sample. Because the two OBS recorded the same voltage (see Figure S7 in Supporting Information S1), their data were combined to create a single calibration curve for each site (Section S3 in Supporting Information S1). Erosion rate, E, was estimated from a linear fit of voltage versus time when erosion was occurring, which spanned 100–300 s (e.g., Figure S7 in Supporting Information S1). The site-specific calibration was used to convert voltage rate of change to erosion rate.

After the erosion experiment for each side of a given core was completed, a Nortek Vectrino was used to record instantaneous velocity in the streamwise, $u(t)$, lateral, $v(t)$, and vertical, $w(t)$, directions at two pump settings (30 and 60 Hz). A five-point lateral profile was made at mid-depth across the downstream end of the core. Because of the constraints of the Vectrino prongs, velocity was not measured within 3 cm of the wall, and the lateral profile was limited to the central 4 cm of the channel. Vertical profiles of velocity and TKE were uniform, such that lateral profiles at a single location were sufficient. The lateral-average of five ADV measurements at mid-depth (U_{ADV}) agreed with the channel-average U_o to within 13%, with $U_o/U_{ADV} = 1.04 \pm 0.13$ (SD). At each position, velocity was measured at 200 Hz for 60 s, which was sufficient to capture mean and turbulent velocity statistics based on convergence tests with longer records. Each record was decomposed into time-average ($\overline{u}, \overline{v}, \overline{w}$) and fluctuating ($u'(t), v'(t), w'(t)$) components. The data was processed using the Goring and Nikora (2002) method to remove spikes, with the acceleration and velocity thresholds set to $\lambda = 1$ and $k = 1.5$, respectively. The TKE per fluid mass $\left(\frac{1}{2}(\overline{u'^2} + \overline{v'^2} + \overline{w'^2})\right)$ was laterally averaged and defined as k_t.

For each bare core, the bed shear stress, τ_b, was estimated by extrapolating a vertical profile of Reynolds stress to the bed, from which a bed stress coefficient $C_f = \tau_b/\rho U_o^2$ was defined. For each site the average of four measurements were used to define the mean and SE (see Table 1). For cores with pneumatophores, the Reynolds stress profile did not provide a good estimate of bed stress (see Figure S8 in Supporting Information S1), as discussed in previous studies (e.g., Nepf, 2012; Yang et al., 2016). Instead, for cores with pneumatophores the bed stress was estimated using the following model developed by Conde-Frias et al. (2023) that estimates the enhancement of bed shear stress by vegetation-generated turbulence, when this effect is present,

$$\tau_b = \rho \left(\max \left(K \sqrt{\frac{k_t}{Re_d}}, \sqrt{C_f}\, U_o \right) \right)^2 \qquad (1)$$

in which $K = 9.5 \pm 0.4$ is a scale constant, and ρ is the water density. $Re_d = \frac{U_o d}{\nu(1-\phi)}$ is the stem Reynolds number, in which ν is the kinematic viscosity of water. The first term within the brackets of Equation 1 estimates the bed shear stress when vegetation-generated turbulence reduces the thickness of the viscous sub-layer, enhancing the bed stress. The second term estimates the bed shear stress when the vegetation-generated turbulence has no influence and uses the C_f value estimated from bare cases at the same site (Table 1), which was reasonable since the substrate was the same. The first term is important at low velocity (low Re_d) or high SVF (producing high k_t). In conditions considered here, Equation 1 estimated that bed stress was enhanced by vegetation turbulence only for $U_o < 9$ cm/s, so that for most conditions $\tau_b = \rho C_f U_o^2$ was the same for sections with and without pneumatophores.

However, recall that in this study and for pneumatophores in general the SVF is less than 5%. For higher stem density the influence of vegetated turbulence on bed shear stress can extend into a higher velocity range (Conde-Frias et al., 2023). Finally, the critical bed shear stress, $\tau_{b,c}$, was estimated as the average between the bed shear stress for which the measured erosion rate first rose above zero and the previous bed shear stress that did not cause erosion. The uncertainty in $\tau_{b,c}$ came from the resolution of velocity steps. The constant odds method was used to propagate uncertainty (Kline & McClintock, 1953).

3. Results

For the same channel velocity, the presence of pneumatophores (squares, Figure 2a) was associated with a higher magnitude of turbulence, compared to conditions without pneumatophores (circles, Figure 2a). Turbulence level increased with increasing SVF, denoted by darker symbol colors in Figure 2a, consistent with theory and previous experimental studies (e.g., Tanino & Nepf, 2008; Tinoco & Coco, 2016). In non-cohesive sediment, root-generated turbulence produces scour holes around individual stems in laboratory studies (e.g., Hongwu et al., 2013; Tinoco & Coco, 2016), and scour holes have been observed around individual pneumatophores in sandy soil near the forest edge (Norris et al., 2021). However, scour holes were not observed for any velocity in this study, which was consistent with observations with cohesive sediment beds (Vignaga et al., 2013). The absence of scour hole formation, a precursor to resuspension (e.g., Hongwu et al., 2013), was one indicator that turbulence had a weaker influence on sediment mobility, compared to non-cohesive sediments.

Within each core type (denoted by symbol), the erosion rate generally increased with increasing turbulence, but this was likely due to the correlation between turbulence and channel velocity (Figure 2a). However, across all core types, there was no discernible dependency on turbulence magnitude (Figure 2b). Further, a critical turbulence threshold for initiating erosion could not be identified in Figure 2b. Instead, erosion rate across all core types collapsed with a single dependency on bed shear stress (Figure 2c), and within uncertainty, the critical bed stress was similar across all core types (Figure 2d).

4. Discussion

Previous studies have shown that vegetation-generated turbulence can enhance bed-shear stress (Conde-Frias et al., 2023), but accounting for this enhancement does not improve the prediction of non-cohesive sediment erosion rates (Xu et al., 2022). Instead, for non-cohesive sediment TKE is a better predictor for both the onset and rate of erosion of non-cohesive sediment within model vegetation (e.g., Tinoco & Coco, 2018; Tseng & Tinoco, 2021; Yang et al., 2016). However, this was not observed in the present study with natural cohesive sediment. Although turbulence was significantly enhanced by the presence of real pneumatophores (Figure 2a), the threshold for erosion could not be related to turbulence magnitude (Figure 2b), and the bed-shear stress was a better predictor of both the erosion rate and erosion threshold (Figures 2c and 2d). Combining observations from the present and previous studies suggested differences in the effectiveness of vegetation-generated turbulence in mobilizing cohesive sediment compared with non-cohesive sediment. We hypothesized that this was related to the different forces resisting resuspension.

To mobilize a non-cohesive grain, hydrodynamic forces must exceed the grain's submerged weight and act long enough to accelerate it into motion (Diplas et al., 2008). The time needed to accelerate a particle with diameter D is the particle relaxation time ($t_R = \rho_p D^2/(18\,\mu)$, with particle density ρ_p and fluid viscosity μ, e.g. Hinds & Zhu, 2022). The fluctuation time scale of turbulence generated by reedy vegetation of diameter d exposed to velocity U is $T \sim 5\,d/U$ (e.g., Poggi et al., 2004). If the fluctuating shear and normal stresses have time scales $T > t_R$, then vegetation-generated turbulence can enhance resuspension. This hypothesis is supported by recent studies with sand beds. Tinoco and Coco (2016) observed that the velocity at which resuspension was triggered decreased as the magnitude of vegetation-generated turbulence increased. Xu et al. (2022) observed that the erosion rate of fine quartz grains was enhanced by turbulence generated by model vegetation. In both studies $T > t_R$ (see details in Table S13 of Supporting Information S1).

In contrast, in the present study, vegetation-generated turbulence had no influence on the velocity threshold at which sediment erosion was initiated or the erosion rate, which we attributed to sediment cohesion derived from EPS biofilm. Although we did not measure EPS concentrations, EPS was expected to be present in our cores, because chlorophyll a (an indicator of EPS, e.g., Taylor et al., 2013; Redzuan & Underwood, 2020), has been
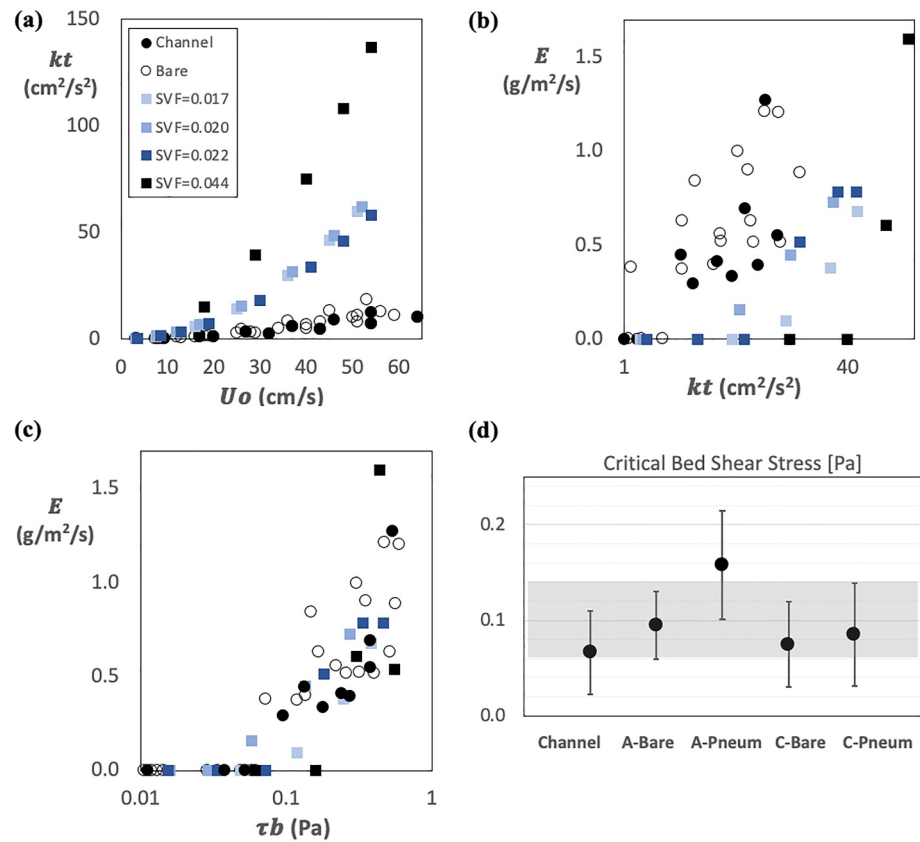
Figure 2. (a) Turbulent kinetic energy (TKE), k_t, versus channel-average velocity, U_0. Blue square markers have lower solid volume fraction (SVF ≈ 0.020), compared to black square markers (SVF = 0.044). (b) Erosion rate, E, vs. TKE, k_t. (c) Erosion rate, E, vs. bed shear stress, τ_b. (d) Critical bed shear stress, $\tau_{b,c}$, for each core type (channel, bare, and with pneumatophores). Shading indicates the average across all core types, with uncertainty.

measured in the sediment at other black mangrove sites in Louisiana. For example, Powell (2018) reported chlorophyll a (chl a) levels of $2.7 \pm 1.8\,\mu$g chl a cm^{-2} at Grand Isle, Louisiana and $1.73 \pm 0.4\,\mu$g chl a cm^{-2} at Bay Champagne, Louisiana. EPS is typically lower in the winter months, which is when we collected the cores, but still present (Dickhudt et al., 2009; Wiberg et al., 2013; Widdows et al., 2004).

EPS biofilm has elastic behavior, that is, stretching before it breaks, such that forces must act for an extended time to break the cohesion. Mechanical tests suggest this requires a time scale of order 10 s (Aggarwal et al., 2010; Ohashi et al., 1999). Similarly, a sediment bed with biofilm cohesion was observed to oscillate before failing, with oscillations on the order of 1 s (video in SI of Vignaga et al., 2013). These time scales suggest that hydrodynamic forces must act for a minimum of 1 to 10 s to either initiate oscillations that weaken the biofilm or directly stretch the biofilm sufficiently to a point of breaking. It is plausible that the time scale of fluctuations associated with pneumatophore-generated turbulence ($T = 5d_{\text{avg}}/U_0 = 0.08$ to 0.6 s) were of insufficient duration to break the biofilm cohesion, which would explain why elevated levels of turbulence associated with the pneumatophores had no impact on the erosion threshold or rate (Figure 2). Similarly, the time scales of vegetation-generated turbulence are too short to mobilize large grains, which have longer relaxation times, $t_R \sim D^2$. This explains why erosion within patches of reedy vegetation has been observed in sand beds (Follett & Nepf, 2012, $D_{50} = 0.5$ mm) but not in gravel beds (Klösch et al., 2018, $D_{50} = 3$ cm).

Another source of cohesion in the mangrove cores was the belowground biomass, especially fine roots, which can enhance soil shear strength (Cahoon et al., 2003; Evans et al., 2022). Several studies have shown that soil shear strength increases with increasing belowground biomass (Sasser et al., 2018; Valentine & Mariotti, 2019). A similar positive correlation between soil shear strength and belowground biomass was observed at our field site

(A. R. Deitrick, 2023). However, the total mass eroded corresponded to a sediment layer thickness less than 1.4 mm, which was too shallow a depth to be strongly influenced by the matrix of belowground roots. Mangrove fine root diameters have been measured in the range of 2.5 mm (McKee et al., 2007) and smaller (Xiong et al., 2017), that is, a single root diameter is comparable in size to the eroded sediment layer.

In the channel cores, but not in the forest cores, we observed infaunal tubes and fecal pellets at the surface (Figure S7 in Supporting Information S1), which suggested additional sources of cohesion in these cores. Specifically, tube-building infauna stimulate microbial growth and bind sediment grains through their mucus production, which enhances sediment cohesion (Clemo et al., 2022; Meadows et al., 1990). Joensuu et al. (2018) found a positive correlation between critical bed shear stress and polychete *Pygospio elegans* (tube-building infauna) density. The stimulation of microbial growth from the tube-building infauna in the channel cores could explain why τ_b and erosion rates were similar between the channel and mangrove cores (Figure 2).

This study suggests that the erosion of cohesive and non-cohesive sediment within vegetated beds follow different trends, which has implications for how sediment transport with vegetation should be represented in models. In 2D depth-averaged models, drag associated with vegetation is represented by an increased bed roughness (e.g., increased bed stress coefficient, Manning's *n* or Chezy coefficient), which effectively enhances the bed shear stress within the model (e.g., Baustian et al., 2018). The enhanced roughness represents the contributions of vegetation form drag in the water column, which produces the vegetation-generated turbulence Tanino and Nepf (2008). In this way, the enhanced bed stress representation within a 2D model indirectly captures the influence of vegetation-generated turbulence on resuspension. This approach is suitable for non-cohesive sediment, for which vegetation-generated turbulence is the main driver of resuspension (Tinoco & Coco, 2016, 2018; Xu et al., 2022). However, it is not suitable for the cohesive sediment considered in this study, for which vegetation-generated turbulence did not influence the rate of resuspension. For cohesive sediment in vegetation, resuspension was better described by the bed shear stress. Therefore, the enhanced bed-stress required within the 2D momentum balance would over-predict the erosion of a cohesive sediment. To represent erosion of cohesive sediment a 2D model must separately estimate an actual bed-stress. This could be achieved by estimating the bed stress coefficient for the substrate ($C_f = f(D_{50}, H)$ for example, using equations 16a or 16c in Julien, 2010) and using it to estimate an actual bed-stress $\tau_b = \rho C_f U_o^2$ from the modeled depth-averaged velocity, U_o. The actual bed-stress would be used to model the erosion of the bed, whereas the influence of vegetation on the momentum balance through form drag would be separately parameterized through the enhanced bed stress representation.

Finally, the critical bed shear stress measured in this study ($\tau_{b,c} = 0.10 \pm 0.05$ Pa) was similar to measurements made in mangrove soils using EROMES (EROsion MEasurement device) ($\tau_{b,c} = 0.1$ to 0.4 Pa, Stokes & Harris, 2015). The EROMES uses a core with small surface area that excludes aboveground biomass. By showing that pneumatophore-generated turbulence had no influence on the critical bed shear stress, these results validate the approach of using sediment cores without aboveground biomass to measure erosion rates in cohesive soils, as in EROMES.

5. Conclusions

This study considered the erosion rate and threshold of natural cohesive sediment retrieved from the interior of a black mangrove forest. For the same channel-average velocity, cores with pneumatophores had elevated TKE compared to cores without pneumatophores, but there was no change in the bed-stress or velocity threshold for sediment erosion or the erosion rate, relative to bare cores without pneumatophores. This differed from results obtained with non-cohesive sediment, for which vegetation-generated turbulence both decreases the threshold for erosion and enhances the rate of erosion. For cohesive sediment, is likely that the short time-scales associated with vegetation-generated turbulence are not of sufficient duration to break the cohesion between grains, which would explain why elevated levels of turbulence associated with the pneumatophores had no impact on the erosion threshold or rate.

Data Availability Statement

The data that supports the findings of this study is available at Figshare (A. Deitrick, 2024) https://doi.org/10.6084/m9.figshare.26099020, and also provided in the Supporting Information File.

References

Abt, S., Clary, W., & Thornton, C. (1994). Sediment deposition and entrapment in vegetated streambeds. *Journal of Irrigation and Drainage Engineering*, *120*(6), 1098–1110. https://doi.org/10.1061/(ASCE)0733-9437(1994)120:6(1098)

Aggarwal, S., Poppele, E., & Hozalski, R. (2010). Development and testing of a novel microcantilever technique for measuring the cohesive strength of intact biofilm. *Biotechnology and Bioengineering*, *105*(5), 924–934. https://doi.org/10.1002/bit.22605

Baustian, M. M., Meselhe, E., Jung, H., Sadid, K., Duke-Sylvester, S. M., Visser, J. M., et al. (2018). Development of an Integrated Biophysical Model to represent morphological and ecological processes in a changing deltaic and coastal ecosystem. *Environmental Modelling & Software*, *109*, 402–419. https://doi.org/10.1016/j.envsoft.2018.05.019

Bouma, T., van Duren, L., Temmerman, S., Claverie, T., Blanco-Garcia, A., Ysebaert, T., & Herman, P. (2007). Spatial flow and sedimentation patterns within patches of epibenthic structures: Combining field, flume and modelling experiments. *Continental Shelf Research*, *27*(8), 1020–1045. https://doi.org/10.1016/j.csr.2005.12.019

Cahoon, D. R., Hensel, P., Rybczyk, J., McKee, K. L., Proffitt, C. E., & Perez, B. C. (2003). Mass tree mortality leads to mangrove peat collapse at Bay Islands, Honduras after Hurricane Mitch. *Journal of Ecology*, *91*(6), 1093–1105. https://doi.org/10.1046/j.1365-2745.2003.00841.x

Celik, A. O., Diplas, P., Dancey, C. L., & Valyrakis, M. (2010). Impulse and particle dislodgement under turbulent flow conditions. *Physics of Fluids*, *22*(4), 46601. https://doi.org/10.1063/1.3385433

Clemo, W. C., Giles, K. D., & Dorgan, K. M. (2022). Biological influences on coastal muddy sediment structure following resuspension. *Limnology & Oceanography*, *67*(11), 2466–2482. https://doi.org/10.1002/lno.12213

Conde-Frias, M., Ghisalberti, M., Lowe, R. J., Abdolahpour, M., & Etminan, V. (2023). The near-bed flow structure and bed shear stresses within emergent vegetation. *Water Resources Research*, *59*(4), e2022WR032499. https://doi.org/10.1029/2022WR032499

Costanza, R., d'Arge, R., de Groot, R., Farber, S., Grasso, M., Hannon, B., et al. (1997). The value of the world's ecosystem services and natural capital. *Nature*, *387*(6630), 253–260. https://doi.org/10.1038/387253a0

Cox, J., Paauw, M., Nienhuis, J., Dunn, F., van der Deijl, E., Esposito, C., et al. (2022). A global synthesis of the effectiveness of sedimentation-enhancing strategies for river deltas and estuaries. *Global and Planetary Change*, *214*, 103796. https://doi.org/10.1016/j.gloplacha.2022.103796

Das, S., & Vincent, J. (2009). Mangroves protected villages and reduced death toll during Indian super cyclone. *PNAS*, *106*(18), 7357–7360. https://doi.org/10.1073/pnas.0810440106

Deitrick, A. (2024). Supporting information Deitrick etal 2024 [Dataset]. *figshare*. https://figshare.com/articles/dataset/_/26099020

Deitrick, A., Hovendon, E., Ralston, D., & Nepf, H. (2023). The influence of vegetation-generated turbulence on deposition in emergent canopies. *Frontiers in Marine Science*, *10*, 1266241. https://doi.org/10.3389/fmars.2023.1266241

Deitrick, A. R. (2023). *Erosion and deposition within mangrove forests* SM Thesis. Woods Hole Oceanographic Institution.

Dickhudt, P. J., Friedrichs, C. T., Schaffner, L. C., & Sanford, L. P. (2009). Spatial and temporal variation in cohesive sediment erodibility in the York River Estuary, Eastern USA: A biologically influenced equilibrium modified by seasonal deposition. *Marine Geology*, *267*(3), 128–140. https://doi.org/10.1016/j.margeo.2009.09.009

Diplas, P., Dancey, C. L., Celik, A. O., Valyrakis, M., Greer, K., & Akar, T. (2008). The role of impulse on the initiation of particle movement under turbulent flow conditions. *Science*, *322*(5902), 717–720. https://doi.org/10.1126/science.1158954

Evans, B. R., Brooks, H., Chirol, C., Kirkham, M. K., Möller, I., Royse, K., et al. (2022). Vegetation interactions with geotechnical properties and erodibility of salt marsh sediments. *Estuarine, Coastal and Shelf Science*, *265*, 107713. https://doi.org/10.1016/j.ecss.2021.107713

Follett, E., & Nepf, H. (2012). Sediment patterns near a model patch of reedy emergent vegetation. *Geomorphology*, *179*, 141–151. https://doi.org/10.1016/j.geomorph.2012.08.006

Goring, D. G., & Nikora, V. I. (2002). Despiking acoustic Doppler velocimeter data. *Journal of Hydraulic Engineering*, *128*(1), 117–126. https://doi.org/10.1061/(ASCE)0733-9429(2002)128:1(117)

Grabowski, R. C., Droppo, I. G., & Wharton, G. (2011). Erodibility of cohesive sediment: The importance of sediment properties. *Earth-Science Reviews*, *105*(3), 101–120. https://doi.org/10.1016/j.earscirev.2011.01.008

Hinds, W., & Zhu, Y. (2022). *Aerosol Technology: Properties, behavior, and measurement of airborne particles* (3rd ed.), Wiley & Sons.

Hochard, J. P., Hamilton, S., & Barbier, E. B. (2019). Mangroves shelter coastal economic activity from cyclones. *PNAS*, *116*(25), 12232–12237. https://doi.org/10.1073/pnas.1820067116

Hongwu, T., Wang, H., Liang, D., Lv, S., & Yan, L. (2013). Incipient motion of sediment in the presence of emergent rigid vegetation. *J. Hydro-environ. Res.*, *7*(3), 202–208. https://doi.org/10.1016/j.jher.2012.11.002

Jessup, K., Parker, S. S., Randall, J. M., Cohen, B. S., Jones, R. R., Ganguly, S., & Sourial, J. (2021). Planting stormwater solutions: A methodology for siting nature-based solutions for pollution capture, habitat enhancement, and multiple health benefits. *Urban Forestry and Urban Greening*, *64*, 127300. https://doi.org/10.1016/j.ufug.2021.127300

Joensuu, M., Pilditch, C. A., Harris, R., Hietanen, S., Pettersson, H., & Norkko, A. (2018). Sediment properties, biota, and local habitat structure explain variation in the erodibility of coastal sediments. *Limnology and Oceanography*, *63*(1), 173–186. https://doi.org/10.1002/lno.10622

Julien, P. Y. (2010). *Erosion and sedimentation*. Cambridge University Press.

Kline & McClintok. (1953). The description of uncertainties in a single-sample experiment. *Mechanical Engineering*, *75*, 3–8.

Klösch, M., Busch, E., Gmeiner, P., Glas, M., Haimann, M., Sindelar, C., et al. (2018). The bed shear stress inside and around a circular patch of vegetation. In *Proc. Of the 5th IAHR Europe congress — New challenges in hydraulic Research and engineering editor(s) Aronne Armanini and Elena Nucci*. https://doi.org/10.3850/978-981-11-2731-1_346-cd

Lamb, M. P., de Leeuw, J., Fischer, W. W., Moodie, A. J., Venditti, J. G., Nittrouer, J. A., et al. (2020). Mud in rivers transported as flocculated and suspended bed material. *Nature Geoscience*, *13*(8), 566–570. https://doi.org/10.1038/s41561-020-0602-5

Liu, D., Diplas, P., Fairbanks, J. D., & Hodges, C. C. (2008). An experimental study of flow through rigid vegetation. *Journal of Geophysical Research*, *113*(F4), F04015. https://doi.org/10.1029/2008JF001042

Macreadie, P. I., Costa, M. D. P., Atwood, T. B., Friess, D. A., Kelleway, J. J., Kennedy, H., et al. (2021). Blue carbon as a natural climate solution. *Nature Reviews Earth & Environment*, *2*(12), 12–839. https://doi.org/10.1038/s43017-021-00224-1

McKee, K. L., Rooth, J. E., & Feller, I. C. (2007). Mangrove recruitment after forest disturbance is facilitated by herbaceous species in the Caribbean. *Ecological Applications*, *17*(6), 1678–1693. https://doi.org/10.1890/06-1614.1

Mcleod, E., Chmura, G. L., Bouillon, S., Salm, R., Björk, M., Duarte, C. M., et al. (2011). A blueprint for blue carbon: Toward an improved understanding of the role of vegetated coastal habitats in sequestering CO_2. *Frontiers in Ecology and the Environment*, *9*(10), 552–560. https://doi.org/10.1890/110004

Meadows, P. S., Tait, J., & Hussain, S. A. (1990). Effects of estuarine infauna on sediment stability and particle sedimentation. *Hydrobiologia*, *190*(3), 263–266. https://doi.org/10.1007/BF00008194

Mullarney, J. C., Henderson, S. M., Norris, B. K., Bryan, K. R., Fricke, A. T., Sandwell, D. R., & Culling, D. P. (2017). A question of scale: How turbulence around aerial roots shapes the seabed morphology in mangrove forests of the Mekong delta. *Oceanography*, *30*(3), 34–47. https://doi.org/10.5670/oceanog.2017.312

Narayan, S., Beck, M., Wilson, P., Thomas, C. J., Guerrero, A., Shepard, C. C., et al. (2017). The value of coastal wetlands for flood damage reduction in the Northeastern USA. *Scientific Reports*, *7*(1), 9463. https://doi.org/10.1038/s41598-017-09269-z

Nepf, H. (2012). Hydrodynamics of vegetated channels. *Journal of Hydraulic Research*, *50*(3), 262–279. https://doi.org/10.1080/00221686.2012.696559

Norris, B. K., Mullarney, J. C., Bryan, K. R., & Henderson, S. M. (2021). Relating millimeter-scale turbulence to meter-scale subtidal erosion and accretion across the fringe of a coastal mangrove forest. *Earth Surface Processes and Landforms*, *46*(3), 573–592. https://doi.org/10.1002/esp.5047

Ohashi, A., Koyama, T., Syutsubo, K., & Harada, H. (1999). A novel method for evaluation of biofilm tensile strength resisting erosion. *Water Science and Technology*, *39*(7), 261–268. https://doi.org/10.2166/wst.1999.0367

Packman, A. (2013). Building bacterial bridges. *Nature Geoscience*, *6*(9), 682–683. https://doi.org/10.1038/ngeo1938

Paola, C., Twilley, R. R., Edmonds, D. A., Kim, W., Mohrig, D., Parker, G., et al. (2011). Natural processes in delta restoration: Application to the Mississippi delta. *Annual Review of Marine Science*, *3*(1), 67–91. https://doi.org/10.1146/annurev-marine-120709-142856

Poggi, D., Porporato, A., Ridolfi, L., Albertson, J., & Katul, G. (2004). The effect of vegetation density on canopy sub-layer turbulence. *Bound. Lay. Met.*, *111*(3), 565–587. https://doi.org/10.1023/b:boun.0000016576.05621.73

Powell, C. (2018). *Influence of black mangrove expansion on salt marsh faunal communities of Eastern Coastal Louisiana* Master's thesis. Louisiana State University. https://doi.org/10.31390/gradschool_theses.4633

Redzuan, N. S., & Underwood, G. J. C. (2020). Movement of microphytobenthos and sediment between mudflats and salt marsh during spring tides. *Frontiers in Marine Science*, *7*. https://doi.org/10.3389/fmars.2020.00496

Sasser, C. E., Evers-Hebert, E., Holm, G. O., Milan, B., Sasser, J. B., Peterson, E. F., & DeLaune, R. D. (2018). Relationships of marsh soil strength to belowground vegetation biomass in Louisiana coastal marshes. *Wetlands*, *38*(2), 401–409. https://doi.org/10.1007/s13157-017-0977-2

Stokes, D. J., & Harris, R. J. (2015). Sediment properties and surface Erodibility following a large-scale mangrove (Avicennia marina) removal. *Continental Shelf Research*, *107*, 1–10. https://doi.org/10.1016/j.csr.2015.07.011

Tang, C., Lei, J., & Nepf, H. (2019). The impact of a vegetation-generated turbulence on the critical wave-velocity for sediment resuspension. *Water Resources Research*, *55*(7), 5904–5917. https://doi.org/10.1029/2018WR024335

Tanino, Y., & Nepf, H. M. (2008). Lateral dispersion in random cylinder arrays at high Reynolds number. *Journal of Fluid Mechanics*, *600*, 339–371. https://doi.org/10.1017/S0022112008000505

Taylor, J. D., McKew, B. A., Kuhl, A., McGenity, T. J., & Underwood, G. J. C. (2013). Microphytobenthic Extracellular Polymeric Substances (EPS) in intertidal sediments fuel both generalist and specialist EPS-degrading bacteria. *Limnology & Oceanography*, *58*(4), 1463–1480. https://doi.org/10.4319/lo.2013.58.4.1463

Tinoco, R. O., & Coco, G. (2016). A laboratory study on sediment resuspension within arrays of rigid cylinders. *Advances in Water Resources*, *92*, 1–9. https://doi.org/10.1016/j.advwatres.2016.04.003

Tinoco, R. O., & Coco, G. (2018). Turbulence as the main driver of resuspension in oscillatory flow through vegetation. *Journal of Geophysical Research: Earth Surface*, *123*(5), 891–904. https://doi.org/10.1002/2017JF004504

Tolhurst, T. J., Consalvey, M., & Paterson, D. M. (2008). Changes in cohesive sediment properties associated with the growth of a diatom biofilm. *Hydrobiologia*, *596*(1), 225–239. https://doi.org/10.1007/s10750-007-9099-9

Tseng, C. Y., & Tinoco, R. O. (2021). A two-layer turbulence-based model to predict suspended sediment concentration in flows with aquatic vegetation. *Geophysical Research Letters*, *48*(3), e2020GL091255. https://doi.org/10.1029/2020GL091255

Valentine, K., & Mariotti, G. (2019). Wind-driven water level fluctuations drive Marsh edge erosion variability in microtidal coastal bays. *Continental Shelf Research*, *176*, 76–89. https://doi.org/10.1016/j.csr.2019.03.002

Valentine, K., Mariotti, G., & Fagherazzi, S. (2014). Repeated erosion of cohesive sediments with biofilms. *Advances in Geosciences*, *39*, 9–14. https://doi.org/10.5194/adgeo-39-9-2014

Vignaga, E., Sloan, D., Luo, X., Haynes, H., Phoenix, V., & Sloan, W. (2013). Erosion of biofilm-bound fluvial sediments. *Nature Geoscience*, *6*(9), 770–774. https://doi.org/10.1038/ngeo1891

Waltham, N., Elliott, M., Lee, S. Y., Lovelock, C., Duarte, C., Buelow, C., et al. (2020). UN decade on ecosystem restoration 2021–2030—What chance for success in restoring coastal ecosystems? *Frontiers in Marine Science*, *7*, 71. https://doi.org/10.3389/fmars.2020.00071

Wiberg, P. L., Law, B. A., Wheatcroft, R. A., Milligan, T. G., & Hill, P. S. (2013). Seasonal variations in erodibility and sediment transport potential in a mesotidal channel-flat complex, Willapa Bay, WA. *Continental Shelf Research*, *60*, S185–S197. https://doi.org/10.1016/j.csr.2012.07.021

Widdows, J., Blauw, A., Heip, C. H. R., Herman, P. M. J., Lucas, C. H., Middelburg, J. J., et al. (2004). Role of physical and biological processes in sediment dynamics of a tidal flat in Westerschelde Estuary, SW Netherlands. *Marine Ecology Progress Series*, *274*, 41–56. https://doi.org/10.3354/meps274041

Widdows, J., Pope, N. D., & Brinsley, M. D. (2008). Effect of Spartina Anglica stems on near-bed hydrodynamics, sediment erodability and morphological changes on an intertidal mudflat. *Marine Ecology Progress Series*, *362*, 45–57. https://doi.org/10.3354/meps07448

Wu, W., Perera, C., Smith, J., & Sanchez, A. (2018). Critical shear stress for erosion of sand and mud mixtures. *Journal of Hydraulic Research*, *56*(1), 96–110. https://doi.org/10.1080/00221686.2017.1300195

Xiong, Y., Liu, X., Guan, W., Liao, B., Chen, Y., Li, M., & Zhong, C. (2017). Fine root functional group-based estimates of fine root production and turnover rate in natural mangrove forests. *Plant and Soil*, *413*(1), 83–95. https://doi.org/10.1007/s11104-016-3082-z

Xu, Y., Li, D., & Nepf, H. (2022). Sediment pickup rate in bare and vegetated channels. *Geophysical Research Letters*, *49*(21), e2022GL101279. https://doi.org/10.1029/2022GL101279

Yang, J. Q., Chung, H., & Nepf, H. M. (2016). The onset of sediment transport in vegetated channels predicted by turbulent kinetic energy. *Geophysical Research Letters*, *43*(21), 11261–11268. https://doi.org/10.1002/2016GL071092

References From the Supporting Information

Amos, C. L., Grant, J., Daborn, G. R., & Black, K. (1992). Sea carousel—A benthic, annular flume. *Estuarine, Coastal and Shelf Science*, *34*(6), 557–577. https://doi.org/10.1016/S0272-7714(05)80062-9

Coastal Protection and Restoration Authority (CPRA) of Louisiana. (2022). Coastwide reference monitoring system-wetlands monitoring data. *Coastal Information Management System (CIMS) database*. Retrieved from http://cims.coastal.louisiana.gov